Steady melting in material extrusion additive manufacturing

 $Austin \ R. \ Colon, \ David \ Owen \ Kazmer \ and \ Amy \ M. \ Peterson$ Department of Plastics Engineering, University of Massachusetts Lowell, Lowell, Massachusetts, USA, and $fon athan \ E. \ Seppala$

Materials Science and Engineering Division, National Institute of Standards and Technology, Gaithersburg, Maryland, USA

Abstract

Purpose – A main cause of defects within material extrusion (MatEx) additive manufacturing is the nonisothermal condition in the hot end, which causes inconsistent extrusion and polymer welding. This paper aims to validate a custom hot end design intended to heat the thermoplastic to form a melt prior to the nozzle and to reduce variability in melt temperature. A full 3D temperature verification methodology for hot ends is also presented.

Design/methodology/approach – Infrared (IR) thermography of steady-state extrusion for varying volumetric flow rates, hot end temperature setpoints and nozzle orifice diameters provides data for model validation. A finite-element model is used to predict the temperature of the extrudate. Model tuning demonstrates the effects of different model assumptions on the simulated melt temperature.

Findings – The experimental results show that the measured temperature and variance are functions of volumetric flow rate, temperature setpoint and the nozzle orifice diameter. Convection to the surrounding air is a primary heat transfer mechanism. The custom hot end brings the melt to its setpoint temperature prior to entering the nozzle.

Originality/value — This work provides a full set of steady-state IR thermography data for various parameter settings. It also provides insight into the performance of a custom hot end designed to improve the robustness of melting in MatEx. Finally, it proposes a strategy for modeling such systems that incorporates the metal components and the air around the system.

Keywords Material extrusion, Fused filament fabrication (FFF), Thermal modeling, Melting, Numerical simulation, Thermoplastic polymers

Paper type Research paper

1. Introduction

Material extrusion (MatEx) additive manufacturing is the most popular additive manufacturing technology (Vyavahare et al., 2020). The process is used in automotive, electronics, medical devices, textiles and many other applications (Vyavahare et al., 2020). The capability of the process to handle a variety of feedstocks in the form of a simple filament, the design flexibility it provides users and the low cost of the equipment contribute to its popularity. Current challenges for MatEx include anisotropic mechanical properties in finished parts (Vyavahare et al., 2020), relatively poor dimensional accuracy between the geometric model and the finished part (Akbaş et al., 2019), limited print speeds due to the capabilities of the equipment (Go et al., 2017) and high dependence of part properties on the process parameters selected by the user (Sun et al., 2008).

In MatEx additive manufacturing, parts are produced by depositing layers of material upon one another. In thermoplastic MatEx, the material must be heated to form a melt for deposition. A melt is achieved by feeding a filament into a hot end, which consists of a hot end body, a heating element and a nozzle in common designs. The hot end body

The current issue and full text archive of this journal is available on Emerald Insight at: https://www.emerald.com/insight/1355-2546.htm



forms the structure that holds the heating element and nozzle (note: in standard hot ends the thermoplastic does not contact the hot end body) (Krishnanand *et al.*, 2021). Nozzles are available in different orifice diameters and are selected to improve print resolution (smaller diameters) and to reduce print times (larger diameters) (Krishnanand *et al.*, 2021; Nienhaus *et al.*, 2019; Tezel and Kovan, 2021).

Because the filament enters the hot end in a nonflowable state (as an amorphous glass or rubber or a semicrystalline solid), there are thermal gradients present across the axial and radial directions. The thermal gradient of interest for this work is in the radial direction, e.g. the center of the melt is cooler than the edges in contact with the nozzle wall. This thermal

© Jonathan E. Seppala (2023).

Portions of this work is supported by the National Science Foundation (NSF) under GOALI Grant No. #1914651 and NIST Science and Technical Research and Services. Any opinions, findings, and conclusions or recommendations expressed in this material are those of the author(s) and do not necessarily reflect the views of the NSF or NIST. The authors also acknowledge Stratasys, Ltd. as the University of Massachusetts (UMass) Lowell team's GOALI partner, and especially Tim Diekmann for his ongoing interest and support.

Since submission of this article, the following author has updated their affiliation: Austin R. Colon is at the Materials Science and Engineering Division, National Institute of Standards and Technology, Gaithersburg, Maryland, USA.

Received 2 June 2023 Revised 4 August 2023 Accepted 4 September 2023

gradient increases as a function of volumetric flow rate and limits the system's maximum volumetric flow rate (Luo et al., 2020; Go et al., 2017). When the maximum volumetric flow rate is surpassed, the material's viscosity is too high and it ceases to flow (Luo et al., 2020; Tlegenov et al., 2017), leading to reductions in interlayer polymer welding and mechanical defects (Gawali and Jain, 2022). The thermal gradient increases as a function of volumetric flow rate because the hot end has a limited heating capacity. The heating capacity is a function of the hot end's geometry (surface area and melting length), composition (type of metal) and heating element (shape and power).

Because of the variability in the process and final part properties due to thermal gradients, researchers have modeled the heat transfer within the MatEx process (Pourali and Peterson, 2019; Xia et al., 2018; Nahar and Gurrala, 2022; Driezen and Herrmann, 2022; Duarte et al., 2021) and implemented models to predict the strength of the welds within the process (Coogan and Kazmer, 2020; Peterson and Kazmer, 2022). As part of those efforts, researchers have investigated modeling of the melt temperature within the MatEx hot end (Trofimov et al., 2022; Xia et al., 2018; Osswald et al., 2018; Moretti et al., 2021; Prajapati et al., 2018; Van Waeleghem et al., 2022; Serdeczny et al., 2020b; Kattinger et al., 2022; Go et al., 2017; Mazzei Capote et al., 2021; Luo et al., 2020; Serdeczny et al., 2022). Models range from simpler analytical models (Phan et al., 2018) to numerical models that leverage axisymmetric assumptions (Nzebuka et al., 2022). Varying assumptions are made. These include whether the melt forms in the nozzle contraction zone or upstream (Osswald et al., 2018; Serdeczny et al., 2020b), Newtonian and non-Newtonian fluid behavior (Van Waeleghem et al., 2022) and variable thermal properties (Nzebuka et al., 2022). For most of these works, the most common hot end design (Krishnanand et al., 2021) is assumed, though some researchers have investigated different designs (Serdeczny et al., 2022).

There are studies that show model validation data for different volumetric flow rates and temperature setpoints, and some have investigated the effect of nozzle orifice diameter/design (Nzebuka et al., 2022; Serdeczny et al., 2022). In most cases, the pressure required to extrude material is the metric for model validation (Serdeczny et al., 2022; Osswald et al., 2018; Mazzei Capote et al., 2021; Serdeczny et al., 2020b; Kattinger et al., 2022). Infrared (IR) thermography has been used to validate models of the melt temperature at the exit of the nozzle for standard hot ends (Roy et al., 2019; Trofimov et al., 2022; Lepoivre et al., 2022; Moretti et al., 2021), though a full set of thermography data has not been used to validate a melting model. In most works, the nozzle is stationary over a print bed when the measurements are taken (Serdeczny et al., 2020a; Prajapati et al., 2018).

In this work, melt formation in a custom hot end is characterized via IR thermography while extruding onto a conveyor at varying experimental conditions. A custom hot end is implemented with the intent of increasing the melting capacity of the system. A conveyor is implemented to enable steady-state measurements at high volumetric flow rates. Simulations of the melt are presented for a one-factor-at-a-time study. The volumetric flow rate, temperature setpoint and nozzle orifice diameter are varied and an acrylonitrile butadiene styrene (ABS) filament is used. The experimental measurements show that volumetric flow rate, temperature

setpoint and the nozzle orifice diameter all influence the measured temperature and the trends observed. A simulation is developed and tuned to provide a methodology for assessment of other hot end designs.

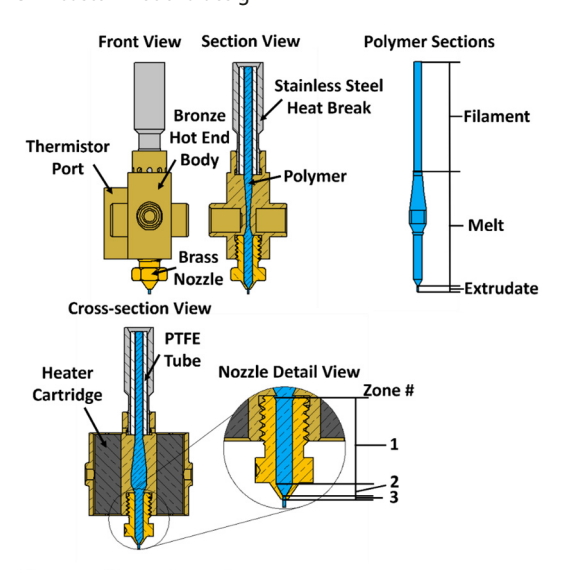
2. Methodology [1]

2.1 Model validation hardware

To validate the modeled temperature, this work uses data from a custom test cell. This test cell consists of a stationary printhead over a conveyor, instrumented to measure the force to feed the filament into the hot end. The hot end is a custom design and is shown in Figure 1. The internal flow bore of the hot end body provided a loft transitioning from a circular bore to a rounded slit and back to enhance the melting of the thermoplastic. Specifically, the design provides a long, tapered transition zone while increasing the surface area and decreasing the thickness of the flow channel. This design is heated by two 40 W heater cartridges on opposite sides of the flow channel, compared to only one heater in common designs. Standard V6 design nozzles (McMaster-Carr part numbers 3695N301, 3695N304, 3695N306, Elmhurst, IL) are threaded into the hot end body. In the instrumentation, an optical camera is positioned in the print direction and an IR camera (FLIR, Wilsonville, OR, model no. A6701sc) is positioned perpendicular to the print direction. The IR camera has a resolution of 640 pixels by 512 pixels, 50 mm lens, 19.05 mm extender ring and a spectral range of $3.0 \,\mu\text{m}$ to $5.0 \,\mu\text{m}$. The spectral range is further limited with a 3900 nm notch filter with 400 nm bandwidth (Spectragon BP-3900-200 nm). Both cameras were set to record at a framerate of 30 Hz.

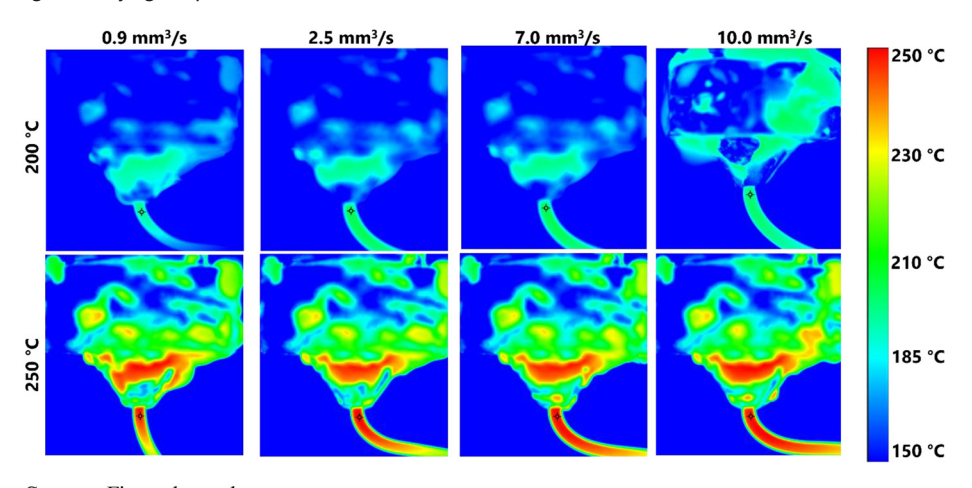
Figure 2 shows sample IR images of the nozzle and the extruded thermoplastic at varying volumetric flow rates and temperature setpoints. The black cursor on each of the images represents a three-pixel by three-pixel square, where the average temperature is measured for the experimental results. This average value across the cursor was averaged over 60 frames to assess the steady-state temperature measurement for each condition. The standard deviation was also calculated

Figure 1 Custom hot end design



Source: Figure by authors

Figure 2 Sample IR images at varying temperatures and volumetric flow rates for a 0.40 mm nozzle diameter



Source: Figure by authors

across the frames as a measure of temperature consistency. The data from these experiments are stored at the National Institute of Standards and Technology, and information for accessing the data is provided in the supplemental materials Section S.1.

2.2 Experiment for model validation

The material of choice is an ABS (Hatchbox ABS, black, 1.75 mm diameter) filament, which was selected for its popularity in the literature (Peterson, 2019). Details of the material are provided in supplemental materials Section S.2. To characterize the MatEx process, the volumetric flow rate, temperature setpoint and the nozzle orifice diameter are varied in a design of experiments defined in supplementary materials Table S.3 (the rationale for selecting the given values is also included in supplementary materials Section S.3). For each parameter combination, a 1-min extrusion is performed with the nozzle 4.0 mm above the conveyor belt. This enables the conveyor to remove the material from the field of view while achieving steady-state conditions.

2.3 Assumptions, boundary conditions and meshing

The geometry of the hot end is modeled first in SolidWorks (Dassault Systemes, Vélizy-Villacoublay, France). This solid model includes the heat break, the hot end body and the nozzle. The thermoplastic filament entering the hot end, the molten material in the hot end and nozzle and the extrudate are also modeled. The air around the hot end is modeled as a cylinder. After modeling the geometry in SolidWorks, it is imported into COMSOL Multiphysics, where the materials and physics are defined. The thermoplastic is assumed to have specific heat, thermal conductivity and density that vary with temperature. For the physics, a nonisothermal flow model is implemented using the laminar flow and heat transfer in COMSOL's solids and fluids modules. The thermoplastic is assumed to be a compressible, generalized Newtonian fluid (with shear-thinning and temperature dependent viscosity) under steady-state laminar flow for these simulations. It is assumed that the melt flows into the hot end through an inlet at a constant velocity profile, defined by the volumetric flow rate and that the outlet is defined as atmospheric pressure (101,325 Pa). It is also assumed that there is a no-slip condition at the flow channel wall.

For heat transfer, it is assumed that there is convectively enhanced conduction within the air (which is achieved by defining a Nusselt number in the conductive heat flux term of the energy conservation equation) (Yungus et al., 2012). Details on the selection of values for the Nusselt number are provided in supplementary materials Section S.5. Viscous dissipation is known to occur in polymer melt flows (Cox and Macosko, 1974), so it was assumed in this system. A constant ambient temperature is assumed on the surface of a cylinder surrounding the hot end. A heat source boundary condition is applied to the heater cartridge geometries in the solid model. The value of the heat rate is set to 80 W, distributed across the surface of the heater cartridge domains, to model the two 40W heater cartridges in the hot end. On the surfaces of the thermistor port, the temperature is set as the temperature setpoint, to simulate the thermistor being at temperature. Thermal contact resistance is assumed between the melt and hot end and between the hot end threads and the threads of the nozzle. Details on contact resistance modeling are in supplemental material Section S.6. The mesh for this simulation is described in supplemental materials Section S.7 and is shown below in Figure 3.

2.4 Model equations

To model the flow of the thermoplastic, COMSOL Multiphysics solves conservation equations for mass, momentum and energy at steady-state (Deen, 2012):

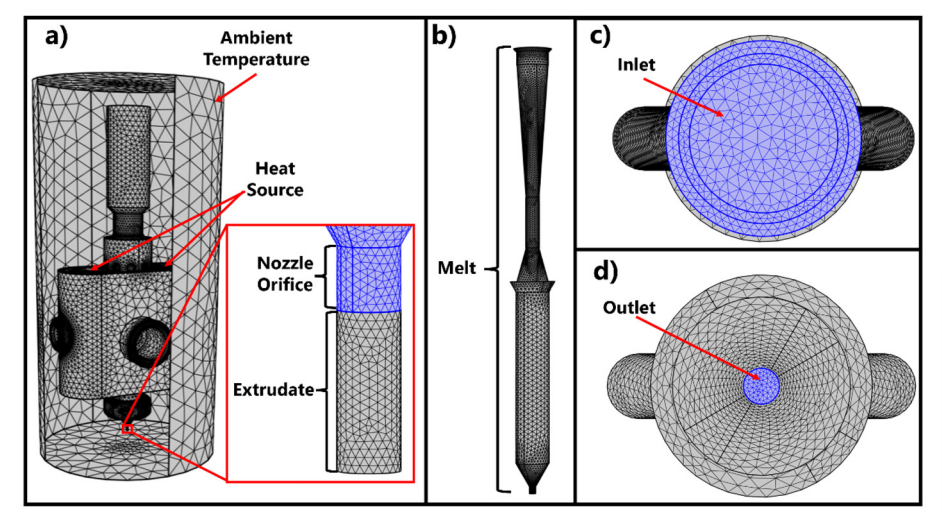
$$\nabla \cdot (\rho \mathbf{u}) = 0 \tag{1}$$

$$\rho(\mathbf{u} \cdot \nabla)\mathbf{u} = \nabla \cdot \left[-p\mathbf{I} + \mu \left(\nabla \mathbf{u} + (\nabla \mathbf{u})^{\mathbf{T}} \right) - (2/3)\mu(\nabla \cdot \mathbf{u})\mathbf{I} \right]$$
(2)

$$\rho C_{p}(\mathbf{u} \cdot \nabla T) + \nabla \cdot (-k\nabla T) = \mathbf{\tau} : \nabla \mathbf{u} - (1/\rho)(\delta \rho/\delta T)T(\mathbf{u} \cdot \nabla p)$$
(3)

where ∇ is the gradient operator, ρ is the density, \boldsymbol{u} is the velocity vector, \boldsymbol{p} is the pressure, \boldsymbol{I} is the identity matrix, μ is the dynamic viscosity, the superscript \boldsymbol{T} indicates the transpose operation, C_p is the specific heat at constant pressure, T is the

Figure 3 Model mesh of (a) the overall geometry, (b) the melt alone, (c) the inlet and (d) the outlet



Source: Figure by authors

temperature, k is the thermal conductivity and τ is the viscous stress tensor. It should be noted that the flow is steady in a Eulerian sense, but not in a Lagrangian approach. The strain rate tensor is defined as:

$$\dot{\gamma} = (1/2) \Big(\nabla \mathbf{u} + (\nabla \mathbf{u})^{\mathbf{T}} \Big) \tag{4}$$

where $\dot{\gamma}$ is the strain rate tensor. The shear rate is defined as the magnitude of the strain rate tensor:

$$\dot{\gamma} = \sqrt{2\dot{\gamma} : \dot{\gamma}}$$
 (5)

For the thermoplastic, the viscous stress tensor is defined by Newton's law of viscosity:

$$\tau = 2\mu\dot{\gamma} \tag{6}$$

For the other domains (the brass, bronze, steel, poly (tetrafluoroethylene) [PTFE] tube, and air, and solid ABS) only the energy equation is considered. The material properties for each domain are used in the equation, respectively. It should be noted that there is no viscous heating or pressure work in these domains. Also, the air domain has convectively enhanced conduction, where the velocity of the material is assumed as zero and a Nusselt number is applied to the conduction term of the energy *equation*.

3. Analysis

Three different metrics are used to characterize the results of the simulations. The first is the average temperature across the extrudate surface. This metric is used to compare the model to the experimental results. The surface average temperature, T_S , across the surface of the extrudate is calculated by:

$$T_{\mathcal{S}} = (1/A_s) \int T dA \tag{7}$$

where A_s is the surface area, T is the temperature and dA is the differential of the area. The number- and velocity-weighted average temperatures are also calculated for the cross section of

the melt immediately before the nozzle exit. These averages are calculated by integrating across a line along the diameter the nozzle at the exit of the nozzle orifice, through a cross section of the melt. A line is used instead of the area of a cross section because the flow profile, both the temperature and velocity, is assumed to be axisymmetric in the nozzle. If the flow were not axisymmetric, a cross-sectional surface average would be more appropriate. These values are calculated to characterize the thermal gradient within the thermoplastic as it is extruded. The number average temperature, T_N , is calculated by the following formula:

$$T_N = (1/X) \int T(x) dx \tag{8}$$

where X is the diameter of the cross section, and dx is the differential of the length along the line. The first two averages are calculated using the line average tool in COMSOL Multiphysics. The velocity-weighted average temperature, T_V , is calculated by the integral tool in COMSOL Multiphysics according to the following equation:

$$T_V = \frac{\int T(r)u(r)rdr}{\int u(r)rdr} \tag{9}$$

where u is the magnitude of the velocity as a function of the radius, r, across the extrudate T_V .

To measure the performance of the custom hot end, a dimensionless temperature, M, is defined by comparing the output temperature to the setpoint temperature relative to the ambient temperature:

$$M = ((T_{average} - T_{ambient})/(T_{setpoint} - T_{ambient})) * 100\%$$
 (10)

where $T_{average}$ is the number average temperature across the cross section of the flow bore, $T_{ambient}$ is the ambient temperature, assumed as 20°C and $T_{setpoint}$ is the setpoint temperature.

4. Results

4.1 Experimental data

The results from the analysis of the IR thermography are shown in Figure 4. Each subplot in Figure 4 is the measured surface temperature of the extrudate (such as Figure 3) versus volumetric flow rate for a different temperature setpoint, with 200°C on the left, 225°C in the middle and the 250°C on the right. Results for three nozzle diameters are shown within the subplots. For all three subplots, the 0.25 mm and 0.40 mm nozzle data for the lowest flow rate show a low temperature relative to that of the middle flow rates, which is unexpected. Supplementary Sections S.8 and S.9 show the measured dimensionless temperatures and the standard deviations of the observed temperatures as a function of volumetric flow rate. The standard deviation tends to increase with volumetric flow rate.

4.2 Model tuning

To tune the model, various assumptions are applied relative to the full model and evaluated for the reference condition with a 0.40 mm nozzle diameter, a temperature setpoint of 225°C and a volumetric flow rate of 10 mm³/s. Each assumption was made to gauge the influence of the model components on the full model. For example, constant thermal properties were assumed as opposed to the variable thermal properties in the full model. The results are tabulated in Table 1 and show that convection in the air domain has the greatest effect on the model's performance, with a 27.3°C temperature increase relative to the full model when it is assumed there is no convection in the air domain. The rest of the assumptions all vary within 2°C of the base model's average surface temperature.

4.3 Parametric study

Results of the parametric study are provided in Table 2 across the range of nozzle diameters, temperature setpoints and flow rate setpoints. T_m and σ_m are the measured surface temperature

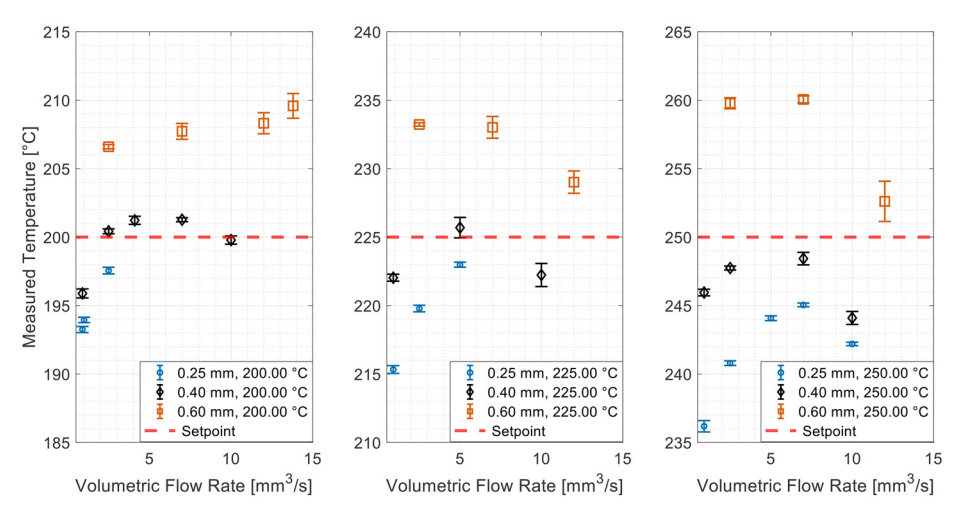
and standard deviation from analysis of IR thermography. Figure 5 shows contour plots of temperature for the parametric study. The order of the plots corresponds with the columns of Table 2. The plots on the left of Figure 5 show a fraction of cold material that increases in size as a function of volumetric flow rate at the entrance of the hot end. The contour plots in the middle of Figure 5 show that the temperature is mostly uniform and that the nozzle orifice diameter has no effect on the temperature of the melt. The righthand set of plots in Figure 5 indicates that there is a cold section of material that reaches the nozzle entrance (about halfway down the melt) at all three temperature setpoints.

Figure 6 shows the average temperature results for the parametric study. For the leftmost plot in Figure 6, the model generally follows the trend of the experimental data, where the low and high volumetric flow rates undershoot the setpoint temperature for the surface average and experimental data and the middle volumetric flow rate is closest to the setpoint temperature. Looking at the middle plot of Figure 6, the temperature predicted by the model does not follow the same trend as the experimental data. The model surface average predicts the temperature to decrease as a function of nozzle orifice diameter, while the experimental temperature increases as a function of nozzle diameter. The middle plot of Figure 6 also shows that nozzle orifice diameter has very little effect on both number average and velocity average temperatures and the model predicts that the temperature would be near its setpoint of 250°C. The rightmost plot of Figure 6 shows the temperature as a function of temperature setpoint. The model does well in predicting the temperature, though there is slightly more error at 200°C, overpredicting the measured temperature that is very close to setpoint temperature.

5. Discussion

Overall, the experiments and simulations comport with most expectations, though there are some critical items, including

Figure 4 Experimentally measured temperature results of IR thermography



Note: The data points are average values, and the error bars represent one standard deviation

taken across 60 frames **Source:** Figure by authors

Table 1 Model tuning for a 0.40-mm nozzle at 225°C and a volumetric flow rate of 10 mm³/s

Assumption	Average surface temperature (°C)
Full model (fewest assumptions)	223.1
Constant thermal properties	222.0
No viscous dissipation	221.5
No convection in the air domain	250.4
No contact resistance between	
melt and wall	224.7
No contact resistance between the	
hot end and the nozzle	223.4
Source: Table by authors	

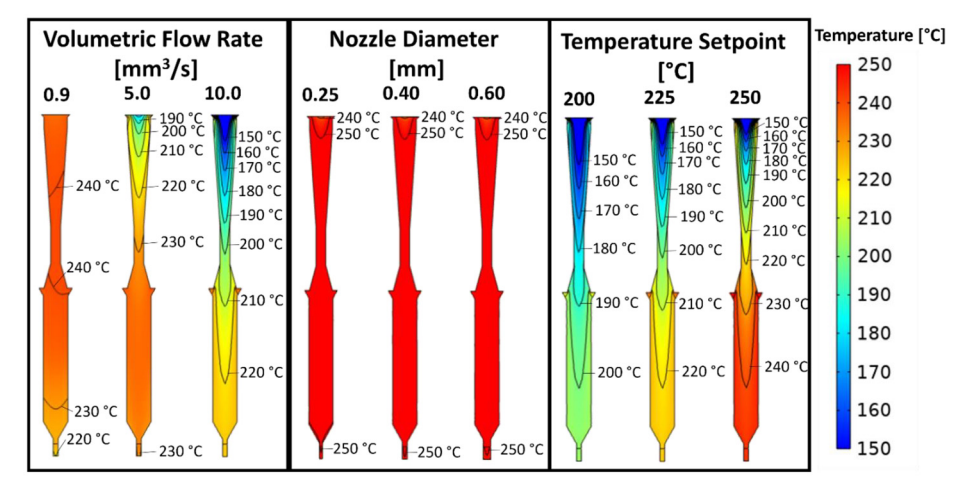
the behavior of the measured temperature as a function of volumetric flow rate and temperature, the ability of the model to replicate the experimentally measured temperature, the effect of nozzle orifice diameter on the measured temperature and the performance of the custom hot end. These items are critical to discuss because the objectives of this work include validating a steady melting model via IR thermography and investigating the performance of the custom hot end design for robust melting.

For the experimental measurements that vary as a function of volumetric flow rate, low volumetric flow rates tend to result in observed extrudate temperatures below the setpoint temperature. This trend is mostly seen in the 0.25 mm and 0.40 mm nozzle orifice diameter data sets and is due to the nozzle being colder than the hot end due to heat convection to the surrounding air. Conversely, at the highest volumetric flow rate, a large amount of material enters the hot end at ambient temperature, but there is inadequate heat transfer and residence time to heat the material to the setpoint temperature. Yet, for the 0.60 mm nozzle at a temperature setpoint of 200°C, the average temperature continues to increase as a function of volumetric flow rate past the volumetric flow rate where the temperature starts to decrease for the 0.40 mm nozzle. This unexpectedly high temperature may be due to viscous dissipation or an uncharacterized error in the IR measurement. To estimate the effect of volumetric flow rate on the viscous dissipation, the volume average viscous dissipation

Table 2 Parametric study results

Condition	1	2	3	4	5	6	7	8	9
Nozzle orifice diameter (mm)	0.4	0.4	0.4	0.25	0.4	0.6	0.4	0.4	0.4
Temperature setpoint (°C)	225	225	225	250	250	250	200	225	250
Volumetric flow rate (mm ³ /s)	0.9	5	10	2.5	2.5	2.5	10	10	10
T _m (°C)	222	225.7	222.2	240.8	247.7	259.8	199.8	222.2	244.1
σ_m (°C)	0.3	0.7	0.8	0.2	0.1	0.4	0.3	0.8	0.5
<i>T_S</i> (° <i>C</i>)	219.3	227.4	223.1	245.5	244.8	243.2	203.7	223.1	242.7
T _N (°C)	226.8	232.1	223.5	250.1	250.7	250.3	203.6	223.5	243.5
$T_V(^{\circ}C)$	226.9	232.4	223.2	250.2	251.1	250.9	203.2	223.2	243.3
M (%)	100.9	103.5	99.3	100.0	100.3	100.1	102.0	99.3	97.2

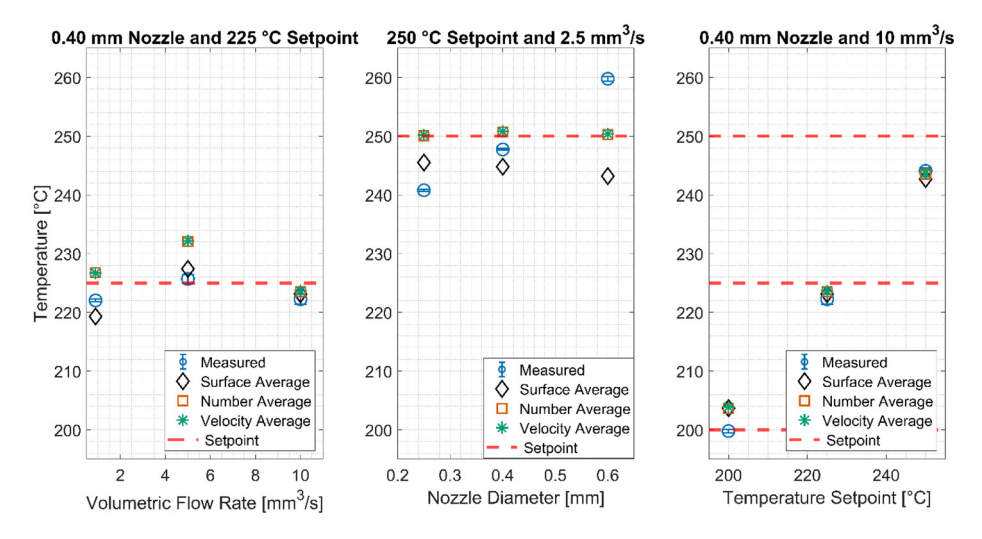
Figure 5 Contour plots of measured temperature versus volumetric flow rate



Note: The left set of contour plots are for a 0.40-mm nozzle orifice diameter and a temperature setpoint of 225°C, the middle set of contour plots are for a temperature setpoint of 250°C and volumetric flow rate of 2.5 mm^{3/s}, and the right set of contour plots are with a 0.40-mm nozzle orifice diameter and a volumetric flow rate of 10 mm^{3/s}

Source: Figure by authors

Figure 6 Parametric study results for the modeled surface average, number average and velocity average temperature



Note: The measured data points are average values, and the error bars represent one standard

deviation

Source: Figure by authors

was calculated for the melt for the low volumetric flow rate and the high volumetric flow rate. The volume average viscous dissipation was found to be 7551 W/m³ for the low volumetric flow rate and 47100 W/m³ for the high volumetric flow rate, showing the amount of viscous dissipation at the high volumetric flow rate is 62 times than at the low volumetric flow rate, making it more significant as volumetric flow rate increases.

When the experimental hot end temperature increases, the overshoot also increases for the 0.60 mm nozzle orifice diameter (see Figure 4). The amount by which the 0.40 mm and the 0.25 mm nozzle orifice diameters fall short of the temperature setpoint also increases as a function of the temperature setpoint. The increasing offset from the temperature setpoint as a function of temperature setpoint likely occurs because convective heat transfer is a function of the temperature difference between the ambient temperature and the temperature of the object, according to Newton's law of cooling. In this case, the extrudate's temperature as it exits the hot end increases as a function of temperature setpoint, leading to a greater rate of heat transfer from the extrudate to the air and the lower temperatures relative to the temperature setpoint. Similar to the results showing the effect of the volumetric flow rate, the simulations are able to replicate the behavior observed for the measured temperature as a function of temperature setpoint.

The measurements taken to study the effect of nozzle orifice diameter on the measured temperature show that the measured temperature increases as a function of the nozzle diameter. This effect was not replicated in the model. This discrepancy is likely due to the difference in curvature of the extrudates at different nozzle diameters. Since the curvature is not accounted for, the amount of incident radiation and the apparent emissivity of the detected object will vary. A study to develop a correction for the IR thermography measured temperatures based on this theory is presented in the supplemental materials [Section S.10, which shows the change in the IR thermography images

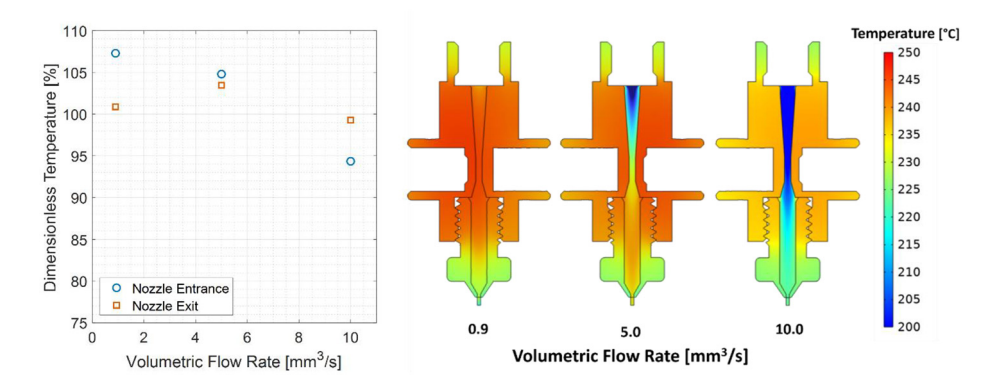
due to nozzle diameter (Figure S.4)]. This work is supported by related IR thermography research (Golzar *et al.*, 2004; Marla *et al.*, 2007).

To evaluate the hot end's performance, the dimensionless temperature is plotted as a function of volumetric flow rate in the left of Figure 7. The dimensionless temperature was calculated prior to the nozzle entrance in the hot end and at the nozzle exit for the model. For the nozzle entrance dimensionless temperature, the number average temperature was calculated across a line along the diameter of the nozzle entrance bore (zone #1 of Figure 1). The results indicate that the temperature of the melt has reached or exceeded the setpoint by the time it reaches the nozzle entrance, and that it maintains that status as it exits the nozzle for the first two flow rates. For the high flow rate, the model indicates that the thermoplastic has only been heated 94% of the way to its setpoint temperature by the time it reaches the nozzle entrance, but almost reaches the setpoint temperature by the time it reaches the nozzle exit.

Figure 7 also provides contour plots of the temperature across the hot end cross section for a nozzle orifice diameter of 0.40 mm, temperature setpoint at 225°C and volumetric flow rates of 0.9, 5 and 10 mm³/s. These plots shows that the metal at the center of the hot end is at a temperature greater than the temperature setpoint, that the temperature of the nozzle is lower than the hot end body's temperature due to heat convection to the surrounding air, and that the nozzle temperature is close to the temperature setpoint. This lower nozzle temperature causes the melt temperature to decrease when it enters the nozzle at a higher temperature for the low volumetric flow rate but causes the temperature to increase when it enters the nozzle at a lower temperature for the high volumetric flow rate conditions.

Based on the predicted dimensionless temperature, with the minimum value by the exit of the nozzle being 99% at the high flow rate, the increased surface area for heat transfer and

Figure 7 Dimensionless temperature for a nozzle orifice diameter of 0.40 mm and a temperature setpoint of 225°C and volumetric flow rates of 0.9, 5 and 10 mm³/s (left) and hot end contour plot demonstrating thermal gradient along the nozzle for the same conditions (right)



Source: Figure by authors

residence time of the melt in the custom hot end provide a robust design for improved melting. However, there still could be some improvement since the dimensionless temperature is not quite at 100%. This could be achieved by increasing the surface area or residence time (length of the hot end flow bore). Additionally, the nozzle face could be covered in an insulating material, or have its surface area minimized, to counteract the heat transfer due to convection with the air. That being said, the custom hot end design shows better performance than a typical hot end design (see supplementary materials Section S.11). Hot end performance is critical because it affects the systems energy efficiency (Kazmer et al., 2023) and the material properties (Kazmer et al., 2021; Kim et al., 2021), which affect the final part's properties.

6. Conclusions

An instrumented test cell was developed to bring the extrudate temperature is brought to steady-state by extruding onto a conveyor, after which it was measured via an IR camera and then modeled via various heat transfer simulations. The experimental results show that the measured temperature of the extrudate varies as a function of the volumetric flow rate, nozzle diameter and the temperature setpoint. The measured temperature is found to be lower than the setpoint at the low volumetric flow rates and high volumetric flow rates. It is also found to increase as a function of nozzle orifice diameter and temperature setpoint.

A 3D simulation of the system is developed, including the metal hot end body and nozzle, heater cartridges, heat break, PTFE tube and an air domain. It was tuned to show the effects of different assumptions, with convection in the air having the greatest influence on the predicted temperature. A parametric study to evaluate the model showed that the temperatures predicted are in good agreement with the experimental results when investigated as a function of volumetric flow rate and temperature setpoint but did not show good agreement as a function of nozzle diameter. The disagreement may be due to the curvature effect on emitted IR radiation for objects of the same temperature. The number average and velocity — weighted average temperatures show the nonisothermal

condition at high flow rates, where the center of the melt is colder than the surface. Still, these values show similar trends as the experimental data for the volumetric flow rate and the temperature setpoint, but do not match the trend of the nozzle orifice diameter data.

The hot end design is also evaluated for its dimensionless temperature and shows promising results relative to typical designs. This modeling technique allows for the design to be evaluated for areas of improvement, since it includes the components of the hot end. For this design, decreasing the nozzle surface area exposed to air would likely be beneficial, since it is colder than the hot end body. The model also indicates that increasing the surface area for melting in the flow bore would likely be beneficial. This concept should be further investigated to achieve the highest dimensionless temperature possible while maintaining energy efficiency. This work provides a data set for thermal model validation, investigation of a modeling approach for hot ends and evaluation of the performance of a hot end designed for improved melting.

Note

Certain equipment, instruments, software or materials, commercial or noncommercial, are identified in this paper to specify the experimental procedure adequately. Such identification is not intended to imply recommendation or endorsement of any product or service by the National Institute of Standards and Technology, nor is it intended to imply that the materials or equipment identified are necessarily the best available for the purpose

References

Akbaş, O.E., Hıra, O., Hervan, S.Z., Samankan, S. and Altınkaynak, A. (2019), "Dimensional accuracy of FDM-printed polymer parts", *Rapid Prototyping Journal*, Vol. 26 No. 2, pp. 288-298, doi: 10.1108/rpj-04-2019-0115.

Coogan, T.J. and Kazmer, D.O. (2020), "Prediction of interlayer strength in material extrusion additive manufacturing",

- Additive Manufacturing, Vol. 35, p. 101368, doi: 10.1016/j. addma.2020.101368.
- Cox, H.W. and Macosko, C.W. (1974), "Viscous dissipation in die flows", AIChE Journal, Vol. 20 No. 4, pp. 785-795, doi: 10.1002/aic.690200421.
- Deen, W.M. (Ed.) (2012), Analysis of Transport Phenomena, Oxford University Press, Oxford.
- Driezen, J. and Herrmann, A.S. (2022), "In-situ adaptive thermal simulation method for predicting and avoiding hotspots in material extrusion processes", *Rapid Prototyping Journal*, Vol. 28 No. 8, pp. 1492-1508, doi: 10.1108/rpj-10-2021-0272.
- Duarte, F.M., Covas, J.A. and Da Costa, S.F. (2021), "Predicting the effect of build orientation and process temperatures on the performance of parts made by fused filament fabrication", *Rapid Prototyping Journal*, Vol. 28 No. 4, pp. 704-715, doi: 10.1108/rpj-04-2021-0084.
- Gawali, S.K. and Jain, P.K. (2022), "Optimization of fused filament fabrication process parameters for mechanical responses of weather-resistant polymer (acrylonitrile styrene acrylate)", *Polymer Engineering & Science*, Vol. 63 No. 1, pp. 139-153, doi: 10.1002/pen.26192.
- Go, J., Schiffres, S.N., Stevens, A.G. and Hart, A.J. (2017), "Rate limits of additive manufacturing by fused filament fabrication and guidelines for high-throughput system design", *Additive Manufacturing*, Vol. 16, pp. 1-11, doi: 10.1016/j.addma.2017.03.007.
- Golzar, M., Beyreuther, R., Brünig, H., Tändler, B. and Vogel, R. (2004), "Online temperature measurement and simultaneous diameter estimation of fibers by thermography of the spinline in the melt spinning process", *Advances in Polymer Technology*, Vol. 23 No. 3, pp. 176-185, doi: 10.1002/adv.20008.
- Kattinger, J., Ebinger, T., Kurz, R. and Bonten, C. (2022), "Numerical simulation of the complex flow during material extrusion in fused filament fabrication", *Additive Manufacturing*, Vol. 49, p. 102476, doi: 10.1016/j. addma.2021.102476.
- Kazmer, D.O., Colon, A.R., Peterson, A.M. and Kim, S.K. (2021), "Concurrent characterization of compressibility and viscosity in extrusion-based additive manufacturing of acrylonitrile butadiene styrene with fault diagnoses", *Additive Manufacturing*, Vol. 46, p. 102106, doi: 10.1016/j. addma.2021.102106.
- Kazmer, D., Peterson, A.M., Masato, D., Colon, A.R. and Krantz, J. (2023), "Strategic cost and sustainability analyses of injection molding and material extrusion additive manufacturing", *Polymer Engineering & Science*, Vol. 63 No. 3, pp. 1-16, doi: 10.1002/pen.26256.
- Kim, S.K., Kazmer, D.O., Colon, A.R., Coogan, T.J. and Peterson, A.M. (2021), "Non-Newtonian modeling of contact pressure in fused filament fabrication", *Journal of Rheology*, Vol. 65 No. 1, pp. 27-42, doi: 10.1122/8.0000052.
- Krishnanand, Soni, S. and Taufik, M. (2021), "Design and assembly of fused filament fabrication (FFF) 3D printers", *Materials Today: Proceedings*, Vol. 46, pp. 5233-5241, doi: 10.1016/j.matpr.2020.08.627.
- Lepoivre, A., Boyard, N., Levy, A. and Sobotka, V. (2022), "Methodology to assess interlayer quality in the material extrusion process: a temperature and adhesion prediction on

- a high performance polymer", *Additive Manufacturing*, Vol. 60, p. 103167, doi: 10.1016/j.addma.2022.103167.
- Luo, C., Wang, X., Migler, K.B. and Seppala, J.E. (2020), "Upper bound of feed rates in thermoplastic material extrusion additive manufacturing", *Additive Manufacturing*, Vol. 32, p. 101019, doi: 10.1016/j.addma.2019.101019.
- Marla, V.T., Shambaugh, R.L. and Papavassiliou, D.V. (2007), "Use of an infrared camera for accurate determination of the temperature of polymer filaments", *Industrial & Engineering Chemistry Research*, Vol. 46 No. 1, pp. 336-344, doi: 10.1021/ie060703a.
- Mazzei Capote, G.A., Oehlmann, P.E.V., Blanco Campos, J. C., Hegge, G.R. and Osswald, T.A. (2021), "Trends in force and print speed in material extrusion", *Additive Manufacturing*, Vol. 46, p. 102141, doi: 10.1016/j. addma.2021.102141.
- Moretti, M., Rossi, A. and Senin, N. (2021), "In-process simulation of the extrusion to support optimisation and real-time monitoring in fused filament fabrication", *Additive Manufacturing*, Vol. 38, p. 101817, doi: 10.1016/j. addma.2020.101817.
- Nahar, C. and Gurrala, P.K. (2022), "Transient thermal finiteelement analysis of fused filament fabrication process", *Rapid Prototyping Journal*, Vol. 28 No. 6, pp. 1097-1110, doi: 10.1108/rpj-05-2021-0104.
- Nienhaus, V., Smith, K., Spiehl, D. and Dörsam, E. (2019), "Investigations on nozzle geometry in fused filament fabrication", *Additive Manufacturing*, Vol. 28, pp. 711-718, doi: 10.1016/j.addma.2019.06.019.
- Nzebuka, G.C., Ufodike, C.O., Rahman, A.M., Gwynn, C.M. and Ahmed, M.F. (2022), "Numerical modeling of the effect of nozzle diameter and heat flux on the polymer flow in fused filament fabrication", *Journal of Manufacturing Processes*, Vol. 82, pp. 585-600, doi: 10.1016/j.jmapro.2022.08.029.
- Osswald, T.A., Puentes, J. and Kattinger, J. (2018), "Fused filament fabrication melting model", *Additive Manufacturing*, Vol. 22, pp. 51-59, doi: 10.1016/j.addma.2018.04.030.
- Peterson, A.M. (2019), "Review of acrylonitrile butadiene styrene in fused filament fabrication: a plastics engineering-focused perspective", *Additive Manufacturing*, Vol. 27, pp. 363-371, doi: 10.1016/j.addma.2019.03.030.
- Peterson, A.M. and Kazmer, D.O. (2022), "Predicting mechanical properties of material extrusion additive manufacturing-fabricated structures with limited information", *Scientific Reports*, Vol. 12 No. 1, p. 14736, doi: 10.1038/s41598-022-19053-3.
- Phan, D.D., Swain, Z.R. and Mackay, M.E. (2018), "Rheological and heat transfer effects in fused filament fabrication", *Journal of Rheology*, Vol. 62 No. 5, pp. 1097-1107, doi: 10.1122/1.5022982.
- Pourali, M. and Peterson, A.M. (2019), "Thermal modeling of material extrusion additive manufacturing", *Polymer-Based Additive Manufacturing: Recent Developments*, American Chemical Society, doi: 10.1021/bk-2019-1315.ch007.
- Prajapati, H., Ravoori, D. and Jain, A. (2018), "Measurement and modeling of filament temperature distribution in the standoff gap between nozzle and bed in polymer-based additive manufacturing", *Additive Manufacturing*, Vol. 24, pp. 224-231, doi: 10.1016/j.addma.2018.09.030.

- Roy, M., Yavari, R., Zhou, C., Wodo, O. and Rao, P. (2019), "Prediction and experimental validation of part thermal history in the fused filament fabrication additive manufacturing process", *Journal of Manufacturing Science and Engineering*, Vol. 141 No. 12, p. 121001, doi: 10.1115/1.4045056.
- Serdeczny, M.P., Comminal, R., Pedersen, D.B. and Spangenberg, J. (2020a), "Experimental and analytical study of the polymer melt flow through the hot-end in material extrusion additive manufacturing", *Additive Manufacturing*, Vol. 32, p. 100997, doi: 10.1016/j.addma.2019.100997.
- Serdeczny, M.P., Comminal, R., Mollah, M.T., Pedersen, D. B. and Spangenberg, J. (2020b), "Numerical modeling of the polymer flow through the hot-end in filament-based material extrusion additive manufacturing", *Additive Manufacturing*, Vol. 36, p. 101454, doi: 10.1016/j.addma.2020.101454.
- Serdeczny, M.P., Comminal, R., Mollah, M.T., Pedersen, D. B. and Spangenberg, J. (2022), "Viscoelastic simulation and optimisation of the polymer flow through the hot-end during filament-based material extrusion additive manufacturing", Virtual and Physical Prototyping, Vol. 17 No. 2, pp. 205-219, doi: 10.1080/17452759.2022.2028522.
- Sun, Q., Rizvi, G.M., Bellehumeur, C.T. and Gu, P. (2008), "Effect of processing conditions on the bonding quality of FDM polymer filaments", *Rapid Prototyping Journal*, Vol. 14 No. 2, pp. 72-80, doi: 10.1108/13552540810862028.
- Tezel, T. and Kovan, V. (2021), "Determination of optimum production parameters for 3D printers based on nozzle diameter", *Rapid Prototyping Journal*, Vol. 28 No. 1, pp. 185-194, doi: 10.1108/rpj-08-2020-0185.
- Tlegenov, Y., Wong, Y.S. and Hong, G.S. (2017), "A dynamic model for nozzle clog monitoring in fused deposition modelling", *Rapid Prototyping Journal*, Vol. 23 No. 2, pp. 391-400, doi: 10.1108/rpj-04-2016-0054.

- Trofimov, A., Le Pavic, J., Pautard, S., Therriault, D. and Lévesque, M. (2022), "Experimentally validated modeling of the temperature distribution and the distortion during the fused filament fabrication process", *Additive Manufacturing*, Vol. 54, p. 102693, doi: 10.1016/j.addma.2022.102693.
- Van Waeleghem, T., Marchesini, F.H., Cardon, L. and D'hooge, D.R. (2022), "Melt exit flow modelling and experimental validation for fused filament fabrication: from Newtonian to non-Newtonian effects", *Journal of Manufacturing Processes*, Vol. 77, pp. 138-150, doi: 10.1016/j.jmapro.2022.03.002.
- Vyavahare, S., Teraiya, S., Panghal, D. and Kumar, S. (2020), "Fused deposition modelling: a review", *Rapid Prototyping Journal*, Vol. 26 No. 1, pp. 176-201, doi: 10.1108/rpj-04-2019-0106.
- Xia, H., Lu, J. and Tryggvason, G. (2018), "Fully resolved numerical simulations of fused deposition modeling. Part II solidification, residual stresses and modeling of the nozzle", *Rapid Prototyping Journal*, Vol. 24 No. 6, pp. 973-987, doi: 10.1108/rpj-11-2017-0233.
- Yungus, A.C., Cimbala, J.M. and Turner, R.H. (2012), Fundamentals of Thermal-Fluid Sciences, McGraw-Hill, New York, NY.

Supplementary material

The supplementary material for this article can be found online.

Corresponding author

Jonathan E. Seppala can be contacted at: jonseppala@nist.gov